Using Deep Eutectic Solvent for Conjugation of Fe_3O_4 Nanoparticles onto Graphene Oxide for Water Pollutant Removal

by

Novin Mehrabi [a], Umar Faruq Abdul Haq [a], M. Toufiq Reza [b], and Nirupam Aich[a, *]

[a] *Department of Civil, Structural and Environmental Engineering, University at Buffalo, The State University of New York, Buffalo, NY 14260*

[b] *Department of Biomedical and Chemical Engineering and Sciences, Florida Institute of Technology, Melbourne, FL 32901*

[*]Corresponding Author: Nirupam Aich, Phone: 716-645-0977, Email: nirupama@buffalo.edu

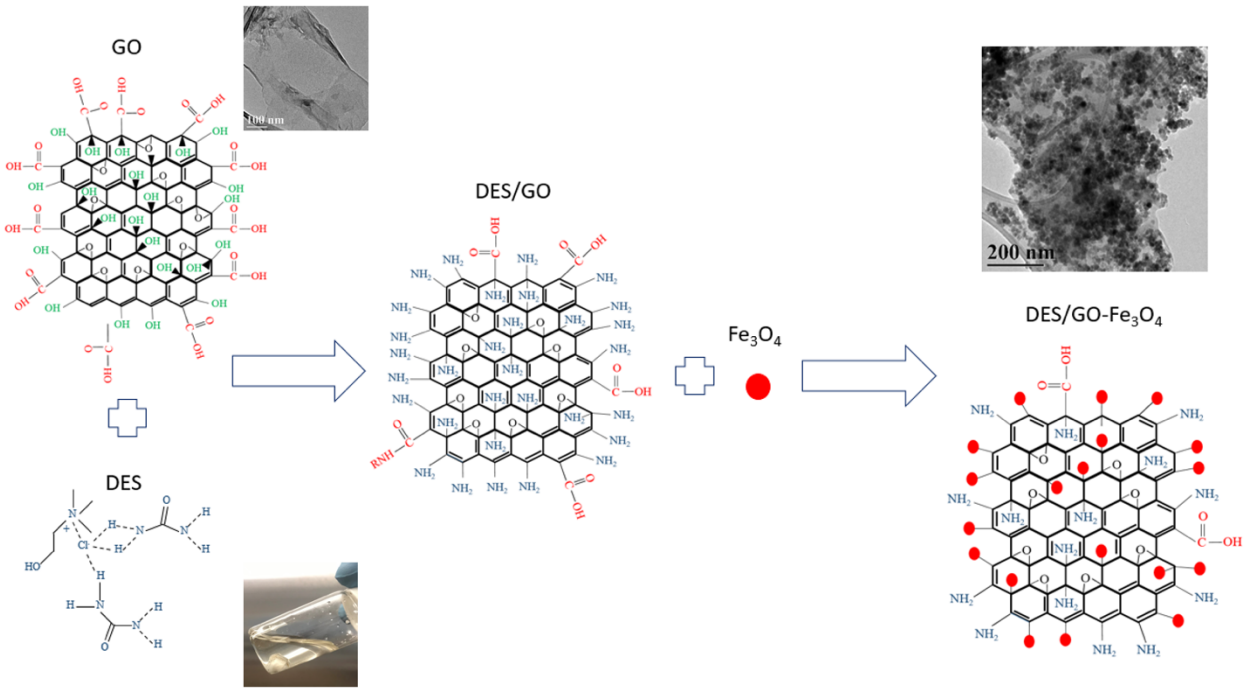
GO
100 nm
DES
DES/GO
Fe3O4
200 nm
DES/GO-Fe3O4

Abstract

Deep eutectic solvents (DESs) have emerged as a substitute for ionic liquids with lower cost and enhanced biodegradability. The most common class of DES refers to a mixture of a quaternary ammonium or phosphonium salt and a hydrogen bond donor (e.g., carboxylic acid) with a melting point lower than that of individual components. DESs have recently shown promise for surface modification of graphene oxide (GO) nanosheets with different functional groups. We hypothesize that such surface functionalization of GO (and other carbon nanomaterials) with DESs can provide a new route to conjugate metallic nanoparticles onto GO surfaces (and similar). Here, we used a typical DES, based on choline chloride and urea, for the conjugation of presynthesized Fe_3O_4 nanoparticles onto GO nanosheets at different GO:Fe_3O_4 ratios. Physicochemical characterization not only confirmed the ability of DES to prepare DES/GO-Fe_3O_4 nanohybrids successfully, but also evidenced the influence of DES on the homogeneity and size distribution of Fe_3O_4 nanoparticles in these nanohybrids. DES/GO-Fe_3O_4 nanohybrids can perform better than both GO and Fe_3O_4 as adsorbents for organic dyes (methylene blue, MB) and heavy metals (Lead (II)). However, depending on the contaminant type, the contaminant removal performance varied differently for DES/GO-Fe_3O_4 nanohybrids with different ratios.

Keywords: ionic liquid, 2D nanomaterials, carbon nanomaterial, water treatment, green synthesis

1. Introduction

Iron-based nanoparticles, including magnetite (Fe_3O_4) nanoparticles, have emerged as one of the most promising technologies for organic and inorganic contaminant removal from water and wastewater (Xu et al., 2012). This can be attributed to their high specific surface area, adsorption and reduction capacity, and ease of recovery and reuse through magnetic separation (Sharififard and Soleimani, 2017). However, in aqueous media, these nanoparticles suffer from loss of surface area and reactivity due to aggregation because of inherently high van der Waals and magnetic attraction forces (Fu et al., 2015; Mehrabi et al., 2019). One way to resolve this issue is to immobilize iron-based nanoparticles onto carbon-based supports including activated carbon, carbon nanotubes, or graphene (Aich et al., 2018; Chen et al., 2016; Masud et al., 2018; Mehrabi et al., 2019). Among the carbon supports, graphene derivatives such as graphene oxide (GO) have emerged as the most promising with its two-dimensional planar surface and high contaminant adsorption capacity for both organic and inorganic pollutants (better than activated carbon and carbon nanotubes) as well as its superior electron transfer capacities for allowing fast redox chemistry (Masud et al., 2018; Mehrabi et al., 2019).

The synthesis of graphene-Fe_3O_4 nanohybrids happens in two major pathways: (i) co-reduction of GO and iron salts (Areerob et al., 2018; Barai et al., 2019) and (ii) attachment of pre-synthesized Fe_3O_4 nanoparticles onto GO nanosheets using chemical bonds (Han et al., 2012; He et al., 2010). The first approach requires either the addition of reducing agents which are mostly harmful chemicals like hydrazine (Chong et al., 2016; Dai et al., 2019; Oh et al., 2015; Thu and Sandhu, 2014) or the use of energy-intensive processes including ultrasonic pyrolysis (Nie et al., 2016). However, these methods allow the attachment of Fe_3O_4 nanoparticles onto GO sheets via weak physical or electrostatic forces, making them susceptible to detachment during the washing or

adsorption process in aqueous media (He et al., 2010). Thus, efforts towards conjugation of GO and Fe_3O_4 using strong bonds have been pursued, but they have mostly required functionalization of Fe_3O_4 nanoparticles with amine-group containing compounds and subsequent usage of coupling agents (Bagherzadeh et al., 2015; Gonzalez-Rodriguez et al., 2019). Large scale synthesis and manufacturing of these graphene-iron nanohybrids calls for faster, low-temperature, and environment-friendly functionalization strategies. The methods should also have the ability to control the size of the iron oxide nanoparticles and prevent their aggregation.

A new class of solvents named deep eutectic solvents (DESs) has emerged as a superior substitute of ionic liquids with similar properties but with much lower cost and toxicity (AlOmar et al., 2016a). DESs are formed when an organic compound – typically a quaternary ammonium or phosphonium salt (hydrogen bond acceptor) – is added to an uncharged hydrogen bond donor (e.g., amines, carboxylic acids, and alcohol) at a ratio to prepare a mixture that has significantly lower melting point (typically less than 100 °C) than the individual components (Li et al., 2018). For example, the most commonly used DES is a mixture of Choline chloride (ChCl, a quaternary ammonium salt) and urea (hydrogen bond donor), prepared at a molar ratio of ChCl:Urea=1:2. Both components are easily available, cheap, and environmentally benign (Khandelwal et al., 2016). DESs present unique properties such as low melting point (Tomé et al., 2018), non-flammability (Smith et al., 2014), low volatility (Smith et al., 2014), chemical and thermal stability (Smith et al., 2014), high solubility (Smith et al., 2014), and biodegradability (Smith et al., 2014) making it a suitable and environmentally green media for materials development with advanced properties for various applications (AlOmar et al., 2017b; Atilhan et al., 2017; Hayyan et al., 2015a; Tomé et al., 2018). The use of DESs has more recently extended to nanomaterial synthesis, processing, and functionalization. The opportunity to have a wide array of possible DES

97 combination along with tunable composition and functionality allows for effective exfoliation of
98 2D nanosheets (Abdelkader and Kinloch, 2016; Abdelkader et al., 2015), functionalization of both
99 carbon and metallic nanomaterials (Atilhan et al., 2017; Hayyan et al., 2015a; Tomé et al., 2018),
100 size- and shape-controlled synthesis of metal nanomaterials (Tomé et al., 2018), and as reaction
101 media (Bozzini et al., 2016; Hammons and Ilavsky, 2017; Tomé et al., 2018). As a
102 functionalization agent, DESs have shown to successfully introduce new functional groups to the
103 surfaces of GO and CNTs surfaces at temperatures as low as 65 °C (Hayyan et al., 2015a).
104 Furthermore, DES functionalized GO and CNT provided higher heavy metal removal due to the
105 introduction of new functional groups and increasing the effective surface area of the adsorbents
106 (AlOmar et al., 2016a; AlOmar et al., 2017a; AlOmar et al., 2016b; AlOmar et al., 2017b).
107 Although few recent literatures showed the surface functionalization of pre-synthesized graphene-
108 iron nanohybrids (synthesized by conventional methods) using DESs for applications in analytical
109 chemistry (Huang et al., 2015), no studies thus far showed the applicability of DESs as a coupling
110 agent for conjugating GO and Fe_3O_4 nanoparticles or any other carbon-metal nanohybrids.
111 Therefore, in this study, we aimed to test the hypothesis that through appropriate amine-
112 functionalization of GO surface using ChCl:Urea DES, we can conjugate the pre-synthesized
113 Fe_3O_4 nanoparticles onto GO surface without the need for any prior-functionalization of Fe_3O_4.
114 The scientific premise of our hypothesis is that Fe_3O_4 nanoparticles have an inherent affinity for
115 amine functional groups, and our DES-functionalized GO surfaces will contain a large amount of
116 amine functional groups (both from ChCl and urea) for sufficient attachment of Fe_3O_4
117 nanoparticles (Mehrabi et al., 2019; Singh and Misra, 2015; Yan et al., 2013). Besides, DES-
118 functionalized GO would obtain more suitable chemistry for hydrogen bond formation between
119 GO and Fe_3O_4. We aim to demonstrate, for the first time, the applicability of DES-derived

graphene-iron nanohybrids for both organic and inorganic pollutants removal from water. To achieve these aims, we first functionalized GO with a DES of ChCl:Urea (2:1) and then subjected to conjugation with Fe_3O_4 to synthesize the DES/GO-Fe_3O_4 nanohybrids with different GO:Fe_3O_4 ratios of 1:1, 1:2, and 1:5. Physical and chemical properties of the synthesized nanohybrids were characterized by transmission electron microscopy (TEM), scanning transmission electron microscopy coupled with energy-dispersive x-ray spectroscopy (STEM/EDS), X-ray diffraction (XRD), and Raman and Fourier transform infrared (FTIR) spectroscopy. The ability of the prepared DES/GO-Fe_3O_4 nanohybrids to remove contaminants from aqueous media was evaluated by performing removal of methylene blue (MB) dye and lead (II), and was compared to the pollutant removal ability of parent materials, i.e., Fe_3O_4 and GO.

2. Material and methods

2.1. Preparation of Fe_3O_4 Nanoparticles

Magnetite (Fe_3O_4) was synthesized based on a well-established method described elsewhere (Ardiyanti et al., 2016). First, Ferric chloride ($FeCl_3$, 97%) and ferrous sulfate heptahydrate ($FeSO_4.7\ H_2O$, >99%) salts were purchased from Fisher Scientific (Hampton, NH). 4.86 g of $FeCl_3$ and 3.34 g of $FeSO_4.7\ H_2O$ were dissolved in 100 mL of deionized (DI) water. Then, the mixture of iron salts and DI water was stirred at 500 rpm using a hotplate magnetic stirrer (Isotemp Advanced Series, Fisher Scientific, Hampton, NH) for 1 h at 55 °C under N_2 gas purge in a 250 mL three-neck flask to achieve a solution containing Fe^{2+} and Fe^{3+} ions. While the solution was being purged by N_2 and mixed by the stirrer, ammonium hydroxide (NH_4OH, 25%, Sigma Aldrich, St. Louis, MO) was added dropwise using a micropipette, until the pH of the solution reached 9.4. This addition of NH_4OH to the iron (Fe^{2+}, Fe^{3+}) solution helped the precipitation of black magnetite (Fe_3O_4) nanoparticles. Then, the solution was left stirring using a mechanical mixer at 500 rpm

for 3 hr. Finally, the Fe_3O_4 nanoparticles were attached to one side of the beaker using a magnet and washed with ethanol and water three times. The obtained Fe_3O_4 nanoparticles were dried at 45 °C under vacuum for 24 h and stored in a glass vial for further use.

2.2. Preparation of the DES solvent

Choline chloride (ChCl, >99%) and Urea (U, ACS Reagent) were purchased from Sigma Aldrich (St. Louis, MO). ChCl was dried overnight at 60 °C in a vacuum oven as it is highly hygroscopic and absorbs humidity quickly. Urea was dried overnight at 90 °C in an air-oven. A solid dry mixture of ChCl:Urea at a molar ratio of 1:2 was placed in a 10 mL vial, and mixed at 60 °C for 3 hrs at 400 rpm using a hotplate magnetic stirrer (Isotemp Advanced Series, Fisher Scientific, Hampton, NH) to prepare the DES solvent (Fig. S1). The solvent was prepared inside a glove box fume hood to avoid any possible change or destruction of the DES properties (Al-Murshedi, 2018). It should be noted that the solid mixture starts liquefying after about 15 min and becomes completely liquid in approximately 3 hrs.

2.3. Preparation of DES/GO-Fe_3O_4 Nanohybrids

Single-layer graphene oxide (GO, > 99.3 wt.%, thickness 0.43-1.23 nm) nanosheets powder was purchased from US Research Nanomaterials, Inc. (Houston, TX). GO powders were placed in an oven overnight at 90 °C to remove its moisture content. Three DES/GO-Fe_3O_4 nanohybrids were prepared with different GO to Fe_3O_4 mass ratios of 1:1, 1:2, and 1:5. For the synthesis of DES/GO-Fe_3O_4 (1:1), 0.1 g of the GO was sonicated for 2 h in 7 mL of DES using a tip sonicator (Q700, Qsonica, Newtown, CT) on a pulse mode (power=50%, on=30 sec, off=5 sec), then 0.1 g of Fe_3O_4 (dried in the vacuum oven at 45 °C for 3 h) was added to the suspension and again sonicated for 1 hr. In the whole process, the suspension temperature was kept at 65 ºC using a water bath with a temperature of 25 °C. Finally, the suspension was stirred at 400 rpm for 2 h at

65 ºC. The synthesized DES/GO-Fe_3O_4 nanohybrids (1:1) were filtered through a 0.2 μm Polyethersulfone membrane (Sterlitech, Kent, WA) and washed three times with ethanol and water. The synthesis steps of DES/GO-Fe_3O_4 nanohybrids are presented briefly as a flowchart in Fig. S2. The obtained nanohybrids were dried overnight in the vacuum oven at 45 °C. In order to synthesize the DES/GO-Fe_3O_4 nanohybrids with the other two ratios of GO and Fe_3O_4 (1:2 and 1:5), the same procedure as above was followed where the total 0.2 g of GO and Fe_3O_4 were dispersed in 7ml DES, but the amounts of GO and Fe_3O_4 were changed to achieve the intended ratios.

2.4. Physicochemical property characterization of DES/GO-Fe_3O_4 nanohybrids

JEOL TEM 2010 transmission electron microscope (TEM, JEOL, Peabody, MA) operating at 200 kV was used to image GO, DES/GO, Fe_3O_4, and DES/GO-Fe_3O_4 nanohybrids to examine their physical morphology and Fe_3O_4 particle size distribution. For the TEM grid preparation, 1 mg of each sample was sonicated in 20 mL of pure ethanol for 30 min using a tip sonicator, followed by placing two drops of the prepared suspension on a carbon-coated copper grid (200 mesh, SPI Supplies, West Chester, PA). The prepared TEM grids were air-dried for at least 30 min at the room temperature before the TEM imaging. The surface morphologies and elemental composition of the samples were studied using a Hitachi SU70 Field Emission Scanning Electron Microscope (FESEM, Hitachi, Japan) at 20 kV coupled with an energy dispersive x-ray spectrometer (EDS, Oxford Instruments, Concord, MA).

Crystal structures of the samples in a powder form were studied using ULTIMA IV X-ray diffractometer (XRD, Rigaku, Wilmington, MA) equipped with Cu laser source at a scanning rate of 2°/min within a range from 5° to 90°. Vibrational frequencies and structural changes of the samples were obtained using a Raman microscope (InVia Qontor, Renishaw, West Dundee,

189 Illinois) with an incident laser wavelength of 514 nm. Functional groups of the parent
190 nanomaterials and the nanohybrids were obtained using a Fourier-transform infrared (FTIR)
191 spectroscopy instrument (1760 FTIR, Perkin-Elmer, Waltham, Massachusetts) in the wavenumber
192 range of 400–3500 cm^{-1}.

193 ***2.5. Methylene blue (MB) and lead(II) adsorption***

194 For MB removal experiments, a 25 mg/L stock solution of MB (Fisher Scientific, Waltham,
195 MA) in DI water was prepared. Different amounts (3, 5, or 10 mg) of the synthesized DES/GO-
196 Fe_3O_4 nanohybrids (1:1, 1:2, 1:5) or their parent nanomaterials (i.e., GO and Fe_3O_4) were placed
197 individually in different 20 mL vials. Then, 10 mL MB solution was poured into each of the vials.
198 The mixture in each vial was bath sonicated for 5 min to provide a suitable contact between MB
199 and the adsorbent (i.e., the nanohybrids or their parent nanomaterials) using a bath sonicator
200 (Branson, 2800, Danbury, CT). Then, a simple ceramic block magnet with dimensions of
201 0.38x0.88x1.88 in^3 (Master magnetics, Castle Rock, CO) was used to separate the adsorbents from
202 the MB solution. MB concentration in each vial after the adsorption was determined by measuring
203 the light absorbance of the solutions at 665 nm wavelength (indicative peak of MB in aqueous
204 solution) using Cary 60 UV-vis spectrophotometer (Agilent, Santa Clara, CA) and comparing the
205 obtained absorbance results with the absorbance of the prepared reference MB solutions. The
206 reported MB removal percentage and standard deviation results were obtained from three identical
207 experiments for each adsorbent dosage.

208 For lead(II) adsorption experiments, four different lead(II) stock solutions with different
209 concentrations of 25, 50, 100, and 150ppm were prepared. 10 mL lead(II) solution of a specific
210 concentration (one from the above) was poured into a 20 mL vial, and 10 mg adsorbent (i.e., the
211 nanohybrids or their parent materials) was added to it. After 5 min of bath sonication to uniformly

disperse the adsorbents in the suspension, the vials were shaken using a mechanical shaker for 48 h at 150 rpm to reach the adsorption equilibrium. Finally, Fe_3O_4 nanoparticles and DES/GO-Fe_3O_4 nanohybrids were separated using the ceramic magnet, while GO was separated by 15 min centrifuge at 10000 rpm using an Eppendorf 5424 centrifuge (Eppendorf, Hauppauge, NY). Lead(II) concentration in the supernatant was measured using Inductively Coupled Plasma Emission Spectrometer (ICP-ES, iCAP 6000, Thermo Scientific, Waltham, MA). A high purity Argon (Ar) gas was used as plasma, auxiliary (0.5 L/min), and nebulizing gas. Before the operation, the ICP-OES was purged with Ar gas for 1 hour. The radio frequency (R.F.) power was kept at 1150 W, and the sample pump rate was fixed at 50 rpm with 5 seconds of stabilization time. For lead(II) content determination, the measurements were observed at the most sensitive emission wavelength for lead(II) at 220.3 nm. A standard calibration curve (R^2 = 0.999) was prepared for known lead(II) concentrations (2, 5, 10, 15, and 20 ppm), which was used to determine the concentration of lead(II) solutions after adsorption by comparing with the light absorption spectrum of the lead(II) solution obtained after adsorbent separation. All the lead (II) adsorption experiments were carried out in triplicates, and the average adsorption capacities along with standard deviations were calculated.

3. Results and Discussion

3.1. Physical morphology and chemical composition of DES/GO-Fe_3O_4 nanohybrids

TEM images of the parent nanomaterials and the synthesized nanohybrids are presented in Fig. 1. For each of the samples, two images are presented, respectively, at low and high magnifications. Fig. 1(a, b) show TEM images of the GO nanosheets, indicating a quasi-transparent single to few layers GO nanosheets. Fig. 1(c, d) show the TEM images of DES functionalized GO nanosheets which we name DES/GO. Compared to GO, DES/GO shows an aggregated structure of GO

nanosheets with wrinkles that may be due to the hydrogen bonds between the amine functional groups after the functionalization of GO nanosheets (Caliman et al., 2018). Fig. 1(e, f) show the TEM images of Fe_3O_4 nanoparticles indicating a chain-like aggregated structure. Fig. 1(g, h), 1(i, j), and 1(k, l) show the TEM images of DES/GO-Fe_3O_4 nanohybrids in a sequence of low-to-high Fe_3O_4 content with GO:Fe_3O_4 ratios of 1:1, 1:2, and 1:5, respectively. It is evident from the figures that Fe_3O_4 nanoparticles are successfully conjugated on the GO substrate with homogenous distribution, and the higher Fe_3O_4 content, the higher Fe_3O_4 accumulation on the GO surface. Since the 30 min of high energy tip sonication for TEM sample preparation was not able to separate the Fe_3O_4 nanoparticles from the GO nanosheets, the conjugation probably happened because of the chemical bonds rendered by DES rather than a simple physical attraction (e.g., van der Waals attraction forces). Further confirmations of the conjugation mechanism for the DES/GO-Fe_3O_4 are provided in the following sections. In order to determine the effects of DES/GO support on controlling the aggregation of Fe_3O_4 nanoparticles, the particle size distribution of individual Fe_3O_4 particles was analyzed for all nanohybrids and bare Fe_3O_4, and the results are presented as histograms in Fig. S3. The average diameters of Fe_3O_4 nanoparticles were 13.6±4.3 nm for the parent Fe_3O_4, 11.9±3.0 nm for DES/GO-Fe_3O_4 (1:1), 11.8±3.1 nm for DES/GO-Fe_3O_4 (1:2), and 12.3±3.5 nm for DES/GO-Fe_3O_4 (1:5). More importantly, the particle size distributions are much narrower for Fe_3O_4 nanoparticles in DES/GO-Fe_3O_4 nanohybrids than bare Fe_3O_4 nanoparticles. The Fe_3O_4 nanoparticles have size ranges of 6-30 nm for bare Fe_3O_4 with significantly right-skewed distribution, 4-22 nm for DES/GO-Fe_3O_4 (1:1) with perfectly normal distribution, 6-22 nm for DES/GO-Fe_3O_4 (1:2) with slightly right-skewed distribution, and 6-26 nm for DES/GO-Fe_3O_4 (1:5) with moderately right-skewed distribution. Therefore, Fe_3O_4 particle sizes in the nanohybrids with low Fe_3O_4 contents (for GO:Fe_3O_4 of 1:1 and 1:2) are smaller and less

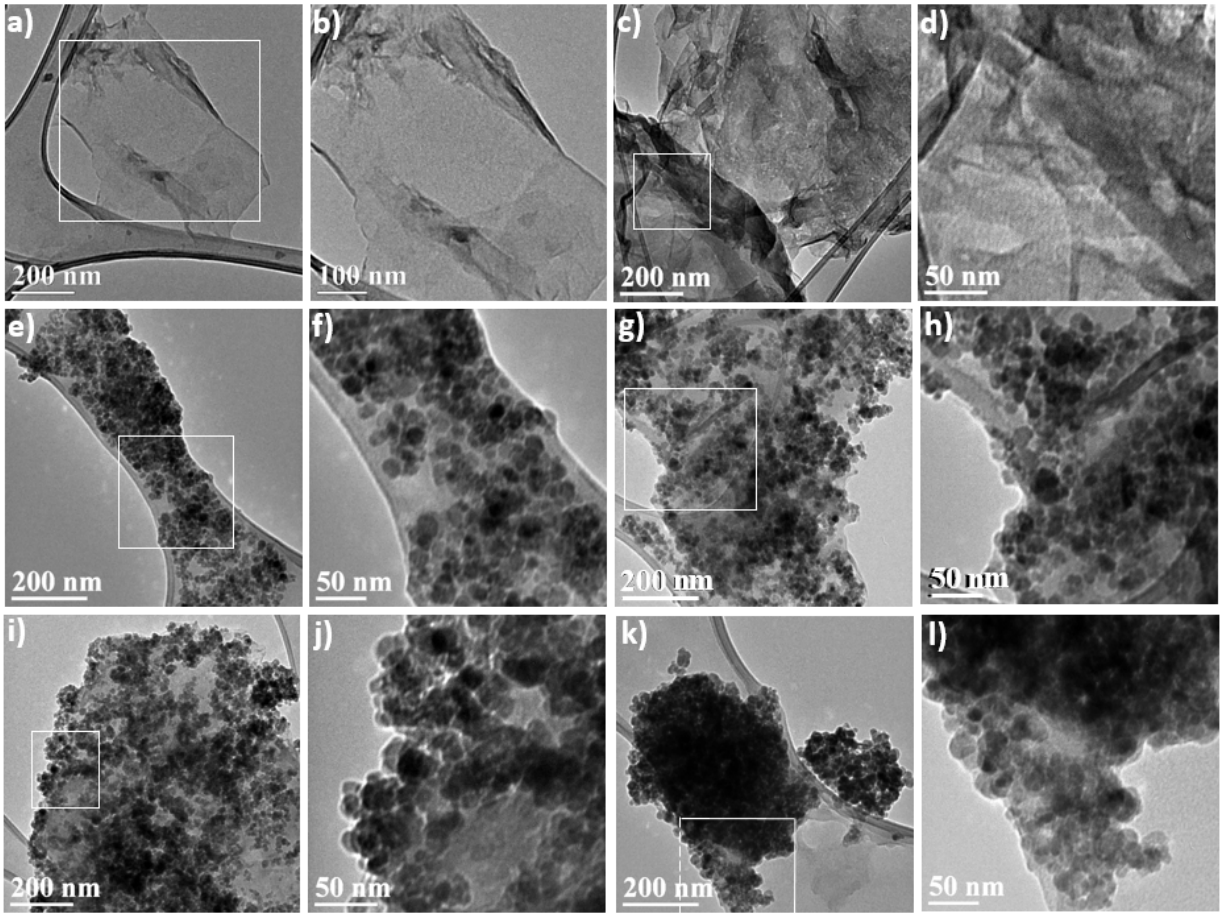

Fig. 1. TEM images of (a, b) GO (c, d) DES/GO (e, f) Fe_3O_4 nanoparticles (g, h) DES/GO-Fe_3O_4 (1:1) (i, j) DES/GO-Fe_3O_4 (1:2), and (k, l) DES/GO-Fe_3O_4 (1:5) nanohybrids.

aggregated compared to the bare Fe_3O_4 particles mainly due to their attachment on the DES/GO as a substrate. By increasing the iron content (DES/GO-Fe_3O_4 (1:5)), Fe_3O_4 nanoparticle sizes on GO nanosheets get closer to the sizes of bare Fe_3O_4 nanoparticles as they start to aggregate (Fig. 1k). Thus, it is evident that using DES as a reaction medium, it is possible to conjugate homogeneously distributed Fe_3O_4 nanoparticles on the GO nanosheets, while the particle size distribution for the deposited Fe_3O_4 nanoparticles can be controlled by changing the GO:Fe_3O_4 ratio.

Fig. 2 shows the surface morphology of the DES/GO-Fe_3O_4 (1:1) nanohybrid along with the EDS elemental maps showing the presence of carbon, nitrogen, oxygen, and iron in the nanohybrid. This indicates the successful conjugation of GO nanosheets and Fe_3O_4 nanoparticles via GO surface modification using DES. Moreover, the elemental maps confirmed the homogeneous distribution of Fe_3O_4 nanoparticles on the GO nanosheets. Fig. S4 presents the surface morphologies of GO and all three nanohybrids along with their corresponding EDS spectra. The SEM image of GO (Fig. S4a) shows the presence of well-distributed nanosheets with defined edges, while SEM images of DES/GO-Fe_3O_4 nanohybrids show more aggregated graphene structures coated with Fe_3O_4 nanoparticles distributed throughout and covering the majority of the surface. EDS spectra show the presence of carbon and oxygen atoms for GO (Fig. S4a), and the presence of carbon, nitrogen, iron, and oxygen atoms for all the synthesized nanohybrids (Figs. S4b-4d) indicating the successful hybridization of GO nanosheets and Fe_3O_4 nanoparticles.

3.2. Crystalline structure of DES/GO-Fe_3O_4 nanohybrids

Fig. 3a presents the XRD spectra of GO, DES/GO, Fe_3O_4, and DES/GO-Fe_3O_4 nanohybrids. The peak around 10° in GO samples confirms the characteristic peak of GO, while this peak was suppressed by the presence of iron nanoparticles in the DES/GO-Fe_3O_4 nanohybrids (Stobinski et al., 2014). After the functionalization of GO with DES, the characteristic peak for carbon shifted to 26°, indicating the reduction of GO by DES without the need for additional reducing agents, which is consistent with previous literature reports (Hayyan et al., 2015a). Furthermore, this broadened peak at 26° indicates DES/GO sheet agglomeration that has been evidenced by TEM images (Fig. 1c and d). The characteristic peaks of magnetite were found at 30.4°, 35.7°,43.5°,

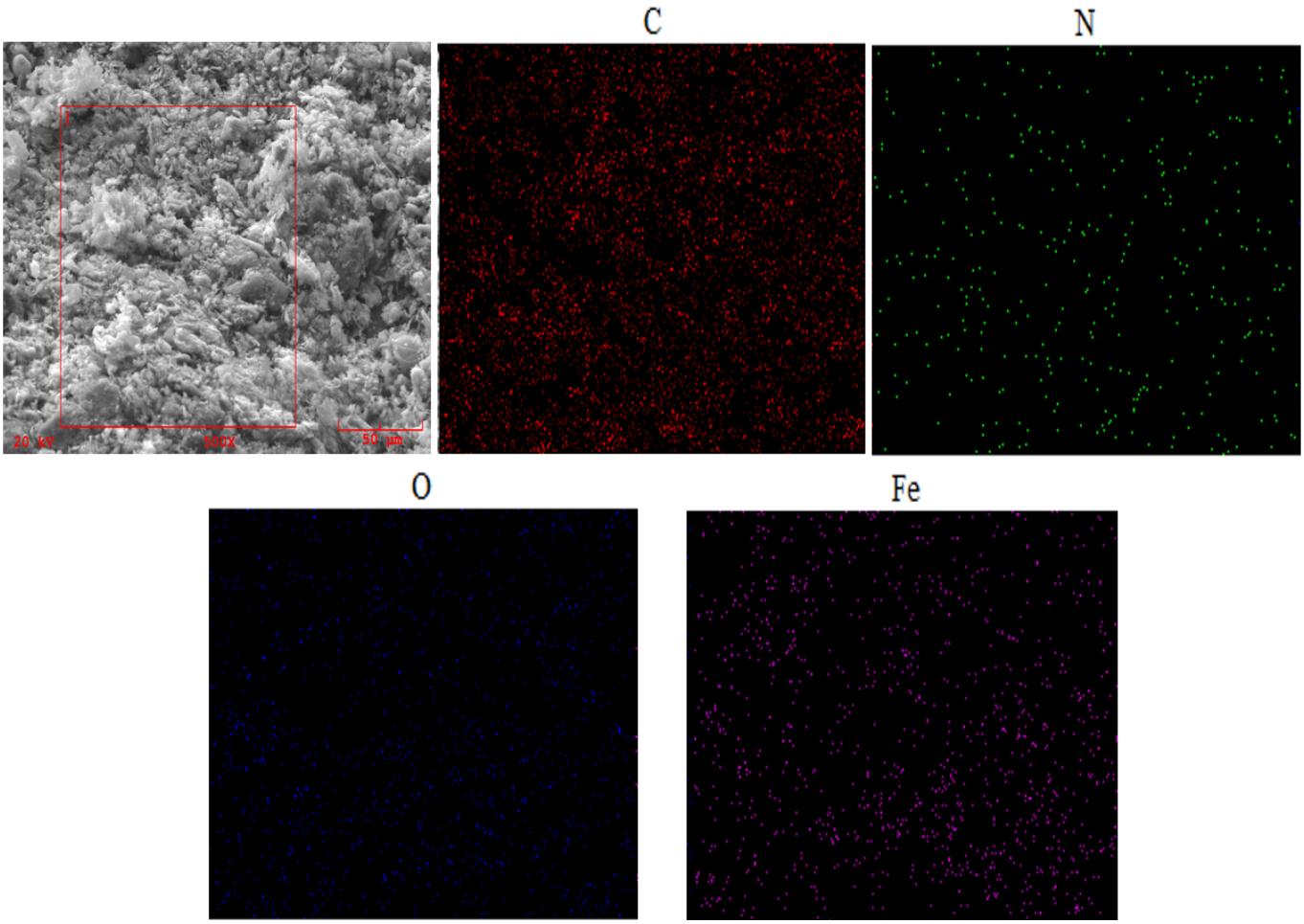

Fig. 2. SEM image and EDS elemental mappings of carbon, nitrogen, oxygen, and iron of DES/GO-Fe_3O_4 (1:1).

53.8°, 57.2°, 63.0°, 71.4°, 74.4°, and 79.1° for the Fe_3O_4 nanoparticle sample (Silva et al., 2013). These characteristics peaks are also seen in the XRD spectra of DES/GO-Fe_3O_4 nanohybrids indicating the successful deposition and conjugation of Fe_3O_4 nanoparticles on the GO nanosheets through DES functionalization. While previous literature reports of XRD results have confirmed the DES functionalization of pre-synthesized GO-Fe_3O_4 nanocomposites for surface modification (Huang et al., 2015), our results for the first time, confirms the use of DES as a coupling agent between GO and Fe_3O_4 nanoparticles for synthesizing the magnetic graphene nanohybrids.

3.3. Molecular vibrations and functional groups of DES/GO-Fe_3O_4 nanohybrids

Fig. 3b shows the Raman spectra of GO, DES/GO, Fe_3O_4, and DES/GO-Fe_3O_4 nanohybrids. Raman shifts at 1605 and 1368 cm^{-1} indicate the characteristic graphitic (G) and defect (D) bands observed in the samples containing GO. After the functionalization of GO with DES, I_D/I_G ratio (an indicator of the defects and disorders in the graphitic matrix) increased from 0.87 to ~1 showing a more disordered carbon structure in DES/GO. A similar increase of the I_D/I_G ratio has been seen previously in the literature for Urea:ChCl modified graphene showing the displacement of oxygen functional groups with other groups (Hayyan et al., 2015a). The I_D/I_G ratio for the DES/GO-Fe_3O_4 nanohybrids increased compared to GO, and DES/GO which corresponds to more defect sites on GO nanosheets created by the deposited Fe_3O_4 nanoparticles – an observation consistent with previous literature reports (Mehrabi et al., 2019; Zhang et al., 2019). However, a decreasing trend in the I_D/I_G ratio is observed for increasing Fe_3O_4 loading in the nanohybrids, which indicates that the defects in structures have been repaired by more Fe_3O_4 nanoparticle coverage at higher Fe_3O_4 loading. Raman shifts at 220, 285, 398, 497, 694, and 1359 cm^{-1} are due to Fe-O stretching vibration (Mehrabi et al., 2019). The presence of Fe-O characteristic shifts in the Raman spectra (although suppressed by GO peaks) of synthesized nanohybrids is another indicator of the successful conjugation of GO and Fe_3O_4 using DES as solvent (Mehrabi et al., 2019).

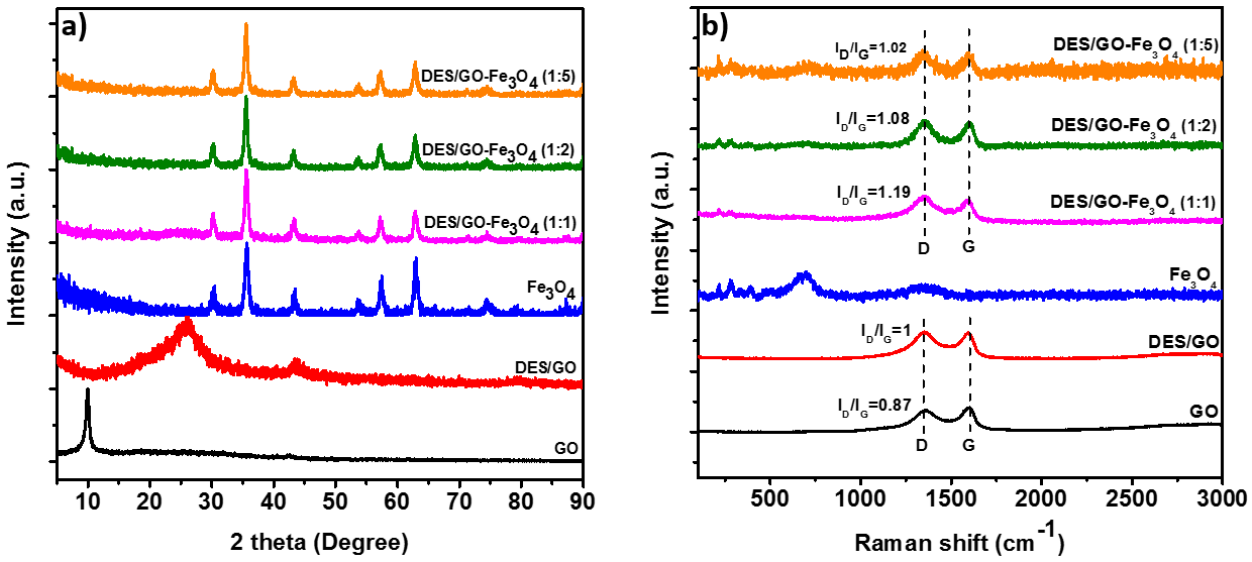

Fig. 3. (a) XRD spectra of GO, DES/GO, Fe_3O_4, DES/GO-Fe_3O_4 (1:1), DES/GO- Fe_3O_4 (1:2), and DES/GO- Fe_3O_4 (1:5) (b) Raman spectra of GO, DES/GO, Fe_3O_4, DES/GO-Fe_3O_4 (1:1), DES/GO-Fe_3O_4 (1:2), and DES/GO-Fe_3O_4 (1:5) nanohybrids

FTIR spectra of GO, DES, and DES/GO are presented in Fig. 4a, and FTIR spectra of Fe_3O_4 and DES/GO-Fe_3O_4 nanohybrids are presented in Fig. 4b. Also, fig. S5 shows all these spectra individually for providing clarity about each peak. The band at 3225 cm^{-1} in all spectra can be assigned to O-H stretching vibrations due to the presence of hydroxyl groups (Caliman et al., 2018). The observed bands at 1724, 1619, 1217, and 1039 cm^{-1} in the GO spectra indicate C=O stretching vibrations of carboxylic acid groups, C=C vibrations from unoxidized graphitic domains, and C-OH and C-O stretching vibrations, respectively (Alzate-Carvajal et al., 2018; Caliman et al., 2018). The spectrum of ChCl:Urea DES shows various characteristic bands including those at 787 cm^{-1} (N-H bond out of plane bending from Urea) (Hayyan et al., 2015a), 867 cm^{-1} (C-N^+ symmetric stretching from ChCl) (Du et al., 2016; Hayyan et al., 2015a), 1436 cm^{-1} (C-N stretching from Urea) (Hayyan et al., 2015a), 1472 cm^{-1} (CH_2 bending from ChCl) (Hayyan et al., 2015a), 1613 cm^{-1} (N-H scissoring from Urea) (Hayyan et al., 2015a), 1661 cm^{-1} (C=O

335 stretching vibration from Urea) (Hayyan et al., 2015a), 3192 cm^{-1} (N-H stretching vibration from
336 ChCl) (Hayyan et al., 2015a) and 3323 cm^{-1} (-NH_2 stretching vibrations from Urea) (Du et al.,
337 2016; Hayyan et al., 2015a). After the functionalization of GO with DES, the carboxylic acid
338 groups peak at 1724 cm^{-1} were weakened which might be due to the partial replacement of
339 carboxylic acid groups by other functional groups (Hayyan et al., 2015a; Huang et al., 2015).
340 Similarly, the O-H stretching vibration at 3225 cm^{-1} for the GO was replaced by N-H stretching
341 vibration at 3192 cm^{-1} and -NH_2 stretching vibration at 3323 cm^{-1}. Besides, new characteristic
342 bands specific to the nitrogen bonding in ChCl:Urea DES appear along with other GO
343 characteristic peaks but overpowering them. The bands at 947, 1436, 1472, 1558, 1661, 3176, and
344 3349 cm^{-1} are attributed to C-N^+, C-N stretching, CH_2 bending, N-H bending vibration, 1° amide
345 N–H scissoring band, N-H stretching vibration, and N-H vibrations, respectively (Alzate-Carvajal
346 et al., 2018; Hayyan et al., 2015a).

347 In the FTIR spectra of Fe_3O_4, the band at 558 cm^{-1} is corresponded to the Fe-O vibration, the
348 bands at 1660, and 3225 cm^{-1} indicate the presence of the hydroxyl groups on the surface of the
349 iron oxide (Yang et al., 2010). The characteristic iron band can also be seen in the FTIR spectra
350 of the DES/GO-Fe_3O_4 nanohybrids indicating the successful conjugation of GO and F_3O_4 using
351 DES as a reaction media (Huang et al., 2015; Mehrabi et al., 2019). Furthermore, the nanohybrids
352 FTIR spectra also show predominant peaks at 1217 cm^{-1} (characteristic C-OH peak of GO), 947
353 cm^{-1} (C-N_+ stretching from DES), 1472 cm^{-1} (CH_2 bending from DES), 1696 cm^{-1} (shifted N-H
354 scissoring band for DES), and 3192 and 3349 cm^{-1} (N-H stretching bands for DES) confirming the
355 conjugation of Fe_3O_4 by coupling through the ChCl:Urea DES.

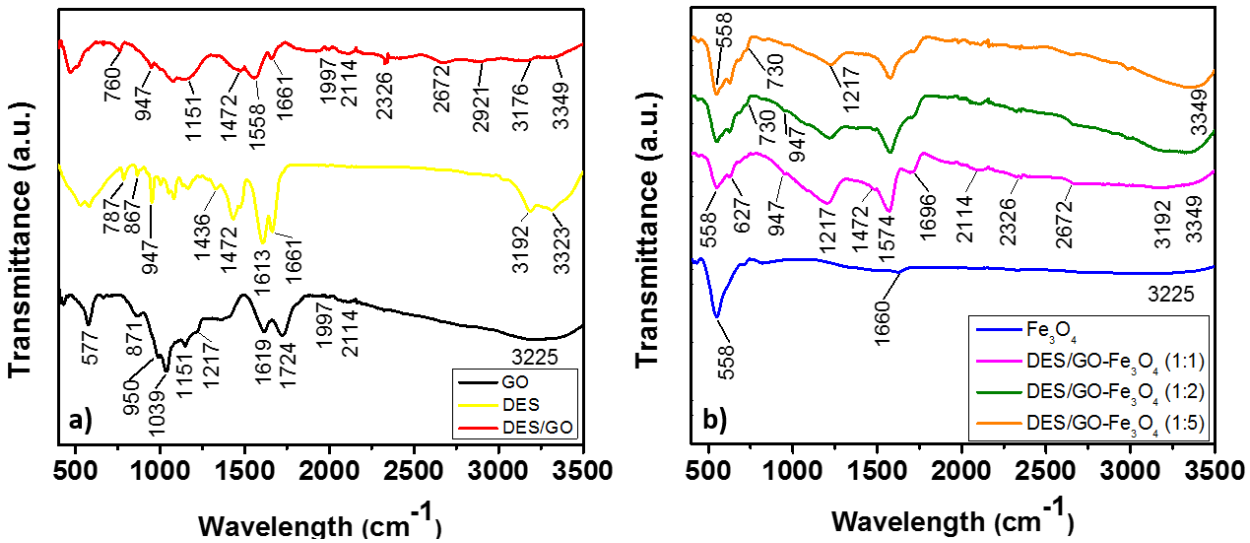

Fig. 4. FTIR spectra of (a) GO, DES, and DES/GO (b) Fe_3O_4 nanoparticles, DES/GO-Fe_3O_4 (1:1), DES/GO-Fe_3O_4 (1:2), and DES/GO-Fe_3O_4 (1:5) nanohybrids.

3.4. Organic dye and heavy metal removal using DES/GO-Fe_3O_4

Fig. 5a presents the MB removal efficiencies of synthesized DES/GO-Fe_3O_4 nanohybrids and their parent nanomaterials as a function of three different dosages of 0.3, 0.5, and 1 mg/mL. Bare Fe_3O_4 nanoparticles could only remove 12.0-30.8% of MB, indicating its limited applicability for MB removal. Such low MB adsorption by bare Fe_3O_4 might be caused due to their aggregation tendencies as evidenced in TEM images. Although GO was able to remove 91.2-93.7% of MB at 0.3-1 mg/mL adsorbent dosages, its separation from water is difficult and needs to be done by centrifuge. At 0.3 mg/mL dosage, DES/GO-Fe_3O_4 nanohybrids with the lowest and highest iron content (GO:Fe_3O_4=1:1 and 1:5, respectively) showed much less MB removal than GO, i.e., only 75.6% and 47.4% MB removal, respectively. However, their MB removal efficiency increased to ~96-98% at 0.5 mg/mL dosage and reached 100% at 1 mg/mL, showing much better performance than GO at high dosages. Most interestingly, DES/GO-Fe_3O_4 (1:2) with the medium iron content showed 100% removal at all three dosages of 0.3, 0.5, and 1 mg/mL presenting this nanohybrid as

372 the most effective and optimum nano-adsorbent for MB removal in this study. The impressive
373 optimization result for MB removal performance of the three nanohybrids indicates the importance
374 of optimizing GO:Fe_3O_4 ratio during conjugation to provide sufficient and homogeneously
375 distributed Fe_3O_4 nanoparticles on the GO sheet. Nevertheless, it is to be noted that all three
376 synthesized DES/GO-Fe_3O_4 nanohybrids were separated from solutions within 5 min by magnetic
377 separation while the GO separation needed 15 min centrifugation time. Furthermore, GO is much
378 more expensive than Fe_3O_4; thus the higher MB removal performance of DES/GO-Fe_3O_4 (1:2)
379 nanohybrid at low dosage, which contains only 33% GO, is indicative of cost minimization
380 through novel nanosorbent generation via DES-coupling.
381 Due to the literature reported limited lead (II) adsorption capacity of Fe_3O_4, we used 1 mg/mL
382 of each nanohybrid and parent nanomaterial for testing lead (II) adsorption. We determined lead
383 (II) adsorption capacity of all the samples as a function of lead (II) concentration, as shown in Fig.
384 5b. Results indicated that DES/GO-Fe_3O_4 nanohybrids were able to remove lead(II) from aqueous
385 solutions more effectively compared to the bare Fe_3O_4. This was probably due to the presence of
386 the GO, functionalization effect of the DES, and the homogenous distribution of the Fe_3O_4
387 nanoparticles in the synthesized nanohybrids. However, at high lead concentrations, nanohybrids
388 with higher iron contents (GO:Fe_3O_4=1:2 and 1:5) showed similar lead (II) adsorption capacity as
389 Fe_3O_4. The maximum lead (II) adsorption capacity of the nanosorbents at the highest lead (II)
390 concentration of 150 mg/L were 120.5±1.3 mg/g for DES/GO-Fe_3O_4 (1:1), 118.14±0.3 mg/g for
391 GO, 73.2±1.7 mg/g for DES/GO-Fe_3O_4 (1:2), 71.1±5.4 mg/g for DES/GO-Fe_3O_4 (1:5), and
392 68.4±5.5 mg/g for Fe_3O_4. Results indicate that the lower the Fe_3O_4 content in the nanohybrids, the
393 higher the lead (II) adsorption capacity. Both GO and DES/GO-Fe_3O_4 (1:1) nanohybrid showed
394 the highest lead (II) adsorption capacity, indicating that the deposition of Fe_3O_4 onto GO at a 1:1

ratio via DES functionalization can improve the adsorption significantly. Similar to MB removal, this provides multiple advantages: i) provides a synergistically enhanced lead (II) adsorption for both GO and Fe_3O_4, (ii) provides magnetic separation capability in the new nanosorbents, and (iii) 50% of the GO can be replaced with much cheaper material Fe_3O_4 to achieve the same level of lead (II) adsorption capacity.

The performance of the newly synthesized DES/GO-Fe_3O_4 nanocomposites was compared with the literature that used nanocomposites based on graphene oxide and iron oxide for adsorption of MB and Lead(II) from water. Tables S1 and S2 show the MB and lead(II) removal presented in the literature with similarly used nanocomposites and operating conditions. Compared to the study results presented in Table S1, our synthesized DES/GO-Fe_3O_4 (1:2) nanohybrid was able to provide the highest MB removal efficiency within a much shorter time (5 min) and at a lower adsorbent dosage (0.3 g/L). For instance, 0.3 g/L of DES/GO-Fe_3O_4 (1:2) was able to remove about 100% of the MB from 25 ppm MB solution while 1 mg/mL of magnetic cellulose/graphene oxide composite was able to remove 96.7% MB from 30 ppm MB solution in 840 min. The same behavior is seen for lead(II) removal by DES/GO-Fe_3O_4 (1:1) nanohybrid. This may be considered as a piece of evidence for the potential of the DES as a solvent for improving the adsorption property of the nanohybrids through physical and chemical modifications.

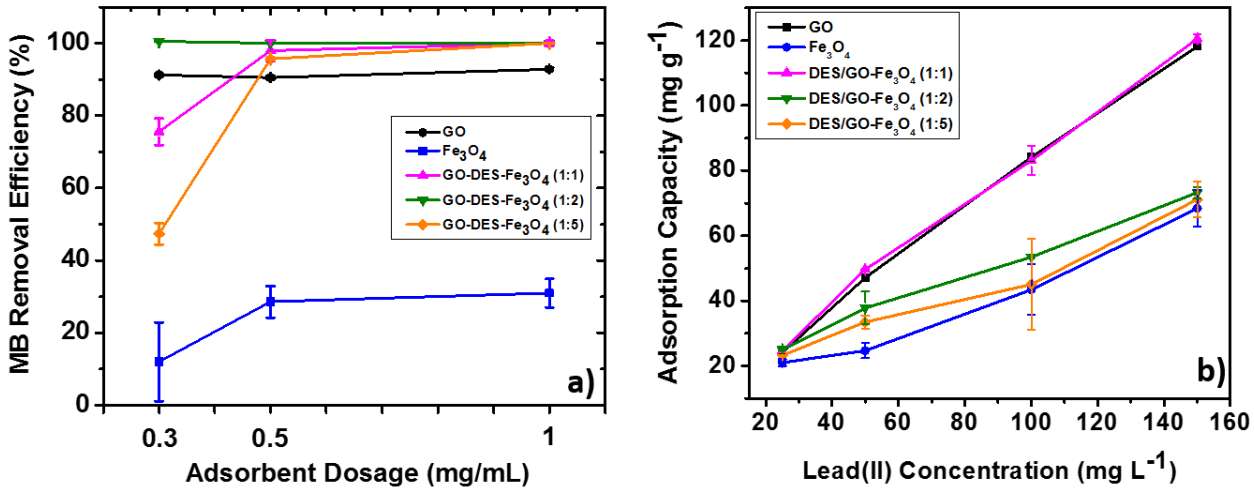

Fig. 5. (a) MB removal from aqueous solution using GO, Fe_3O_4, DES/GO-Fe_3O_4 (1:1), DES/GO-Fe_3O_4 (1:2), and DES/GO-Fe_3O_4 (1:5) (b) Lead(II) removal by GO, Fe_3O_4, DES/GO-Fe_3O_4 (1:1), DES/GO-Fe_3O_4 (1:2) and DES/GO-Fe_3O_4 (1:5).

4. Conclusions

In this study, we successfully utilized a ChCl:Urea based DES as a coupling agent for conjugation of GO nanosheets and Fe_3O_4 nanoparticles at different GO:Fe_3O_4 ratios, as evidenced by the physicochemical property characterization. We used the synthesized novel DES/GO-Fe_3O_4 nanohybrids for the removal of wastewater contaminants, i.e., organic dyes (MB) and heavy metal Lead (II). DES/GO-Fe_3O_4 nanohybrids provide a synergistically enhanced adsorption for both MB and lead (II); however, the adsorption behavior was dependent on the ratio of GO and Fe_3O_4 in the nanohybrid. Among the three nanohybrids with different GO:Fe_3O_4 ratios, DES/GO-Fe_3O_4 (1:2) at the lowest dosage of 0.3 mg/mL showed the best MB removal performance by removing ~100% of 25 mg/L MB within 5 min. Moreover, the maximum adsorption capacity of 120.5±1.3 mg/g Lead (II) at initial Lead (II) concentration of 150 mg/L was obtained by DES/GO-Fe_3O_4 (1:1) nanohybrids with decreasing trend in adsorption capacity with increasing Fe_3O_4 amount in the nanohybrid. We believe that this method of DES functionalization of GO and hybridization with

iron-based nanomaterials can be extended to conjugate other carbon and metallic nanomaterials. Though we used only one type of DES (ChCl:Urea), the availability and wide variety of other DESs are promising for coupling carbon nanomaterials (e.g., GO, CNT) with other metal or metal oxide nanoparticles (e.g., TiO_2, ZnO, Ag, Au) and can be used for various environmental applications via control of the physicochemical properties.

Conflict of Interests

The authors declare that they have no conflict of interests.

Acknowledgments

The authors acknowledge the University at Buffalo's (UB) Furnas Hall Materials Characterization Laboratory, UB Chemistry Department Instrumentation Center, and UB's South Campus Instrument Center for their support with the material characterization.

References

Abdelkader, A. M., Kinloch, I., 2016. Mechanochemical exfoliation of 2D crystals in deep eutectic solvents. ACS Sustain. Chem. Eng. 4**,** 4465-4472.

Abdelkader, A. M., et al., 2015. Electrochemical exfoliation of graphite in quaternary ammonium-based deep eutectic solvents: a route for the mass production of graphane. Nanoscale. 7**,** 11386-11392.

Aich, N., et al., 2018. Application of Nanozerovalent Iron for Water Treatment and Soil Remediation: Emerging Nanohybrid Approach and Environmental Implications. In: Litter M.I. et al. (Ed.,) Iron Nanomaterials for Water and Soil Treatment. Jenny Stanford Publishing, pp. 65-87.

Al-Murshedi A. Y. M., 2018. Deep eutectic solvent-water mixtures. figshare. Thesis. https://hdl.handle.net/2381/42799

AlOmar, M. K., et al., 2016a. Functionalization of CNTs surface with phosphonuim based deep eutectic solvents for arsenic removal from water. Appl. Surf. Sci. 389**,** 216-226.

AlOmar, M. K., et al., 2017a. Allyl triphenyl phosphonium bromide based DES-functionalized carbon nanotubes for the removal of mercury from water. Chemosphere. 167**,** 44-52.

AlOmar, M. K., et al., 2016b. Lead removal from water by choline chloride based deep eutectic solvents functionalized carbon nanotubes. J. Mol. Liq. 222**,** 883-894.

AlOmar, M. K., et al., 2017b. Novel deep eutectic solvent-functionalized carbon nanotubes adsorbent for mercury removal from water. J. Colloid Interf. Sci. 497**,** 413-421.

Alzate-Carvajal, N., et al., 2018. One-step nondestructive functionalization of graphene oxide paper with amines. RSC Adv. 8**,** 15253-15265.

Ardiyanti, H., et al., 2016. Crystal structures and magnetic properties of magnetite (Fe_3O_4)/polyvinyl alcohol (PVA) ribbon. AIP Conf. Proc. 1725, pp. 020007.

Areerob, Y., et al., 2018. Enhanced sonocatalytic degradation of organic dyes from aqueous solutions by novel synthesis of mesoporous Fe_3O_4-graphene/ZnO@SiO_2 nanocomposites. Ultrason. Sonochem. 41**,** 267-278.

Atilhan, M., et al., 2017. Elucidating the Properties of Graphene–Deep Eutectic Solvents Interface. Langmuir 33**,** 5154-5165.

Bagherzadeh, M., et al., 2015. Decoration of Fe_3O_4 magnetic nanoparticles on graphene oxide nanosheets. RSC Adv. 5**,** 105499-105506.

Barai, D. P., et al., 2019. Reduced Graphene Oxide-Fe_3O_4 Nanocomposite Based Nanofluids: Study on Ultrasonic Assisted Synthesis, Thermal Conductivity, Rheology, and Convective Heat Transfer. Ind. Eng. Chem. Res. 58**,** 8349-8369.

Bozzini, B., et al., 2016. Electrochemical fabrication of nanoporous gold decorated with manganese oxide nanowires from eutectic urea/choline chloride ionic liquid. Part III − Electrodeposition of Au–Mn: a study based on in situ Sum-Frequency Generation and Raman spectroscopies. Electrochim. Acta. 218**,** 208-215.

Caliman, C. C., et al., 2018. One-pot synthesis of amine-functionalized graphene oxide by microwave-assisted reactions: an outstanding alternative for supporting materials in supercapacitors. RSC Adv. 8**,** 6136-6145.

Chen, H., et al., 2016. Facile synthesis of graphene nano zero-valent iron composites and their efficient removal of trichloronitromethane from drinking water. Chemosphere 146**,** 32-39.

Chong, S., et al., 2016. Rapid degradation of dyes in water by magnetic Fe0/Fe3O4/graphene composites. J. Environ. Sci. 44**,** 148-157.

Cui, L., et al., 2015. Removal of mercury and methylene blue from aqueous solution by xanthate functionalized magnetic graphene oxide: sorption kinetic and uptake mechanism. J. Colloid Interf. Sci. 439**,** 112-120.

Dai, M., et al., 2019. Magnetic aligned Fe_3O_4-reduced graphene oxide/waterborne polyurethane composites with controllable structure for high microwave absorption capacity. Carbon 152**,** 661-670.

Du, C., et al., 2016. Effect of water presence on choline chloride-2urea ionic liquid and coating platings from the hydrated ionic liquid. Sci. Rep-UK 6**,** 29225.

493 Fu, R., et al., 2015. The removal of chromium (VI) and lead (II) from groundwater using sepiolite-
494 supported nanoscale zero-valent iron (S-NZVI). Chemosphere 138**,** 726-734.
495 Gonzalez-Rodriguez, R., et al., 2019. Multifunctional graphene oxide/iron oxide nanoparticles for
496 magnetic targeted drug delivery dual magnetic resonance/fluorescence imaging and cancer
497 sensing. PLOS ONE 14**,** e0217072.
498 Hammons, J. A., Ilavsky, J., 2017. Surface Pb Nanoparticle Aggregation, Coalescence and
499 Differential Capacitance in a Deep Eutectic Solvent Using a Simultaneous Sample-Rotated Small
500 Angle X-ray Scattering and Electrochemical Methods Approach. Electrochim. Acta 228**,** 462-473.
501 Han, Q., et al., 2012. Facile and tunable fabrication of Fe_3O_4/graphene oxide nanocomposites and
502 their application in the magnetic solid-phase extraction of polycyclic aromatic hydrocarbons from
503 environmental water samples. Talanta 101**,** 388-395.
504 Hayyan, M., et al., 2015a. Functionalization of graphene using deep eutectic solvents. Nanoscale
505 Res. Lett. 10**,** 324.
506 He, F., et al., 2010. The attachment of Fe_3O_4 nanoparticles to graphene oxide by covalent bonding.
507 Carbon 48**,** 3139-3144.
508 Huang, Y., et al., 2015. Magnetic graphene oxide modified with choline chloride-based deep
509 eutectic solvent for the solid-phase extraction of protein. Anal. Chim. Acta. 877**,** 90-99.
510 Kakavandi, B., et al., 2015. Pb (II) adsorption onto a magnetic composite of activated carbon and
511 superparamagnetic Fe_3O_4 nanoparticles: experimental and modeling study. CLEAN–Soil, Air,
512 Water 43**,** 1157-1166.
513 Khandelwal, S., et al., 2016. Deep eutectic solvents (DESs) as eco-friendly and sustainable
514 solvent/catalyst systems in organic transformations. J. Mol. Liq. 215**,** 345-386.

515 Li, X., et al., 2018. Preparation and application of porous materials based on deep eutectic solvents.
516 Cr. Rev. Anal. Chem. 48**,** 73-85.
517 Masud, A., et al., 2018. Shape matters: Cr (VI) removal using iron nanoparticle impregnated 1-D
518 vs 2-D carbon nanohybrids prepared by ultrasonic spray pyrolysis. J. Nanopart. Res. 20**,** 64.
519 Mehrabi, N., et al., 2019. Magnetic graphene oxide-nano zero valent iron (GO–nZVI) nanohybrids
520 synthesized using biocompatible cross-linkers for methylene blue removal. RSC Adv. 9**,** 963-973.
521 Nie, Y., et al., 2016. Crumpled reduced graphene oxide–amine–titanium dioxide nanocomposites
522 for simultaneous carbon dioxide adsorption and photoreduction. Catal. Sci. Technol. 6**,** 6187-6196.
523 Nodeh, H. R., et al., 2015. Magnetic graphene oxide as adsorbent for the removal of lead (II) from
524 water samples. J. Teknol. 78, 25-30.
525 Oh, I., et al., 2015. Deposition of Fe_3O_4 on oxidized activated carbon by hydrazine reducing
526 method for high performance supercapacitor. Microelectron. Reliab. 55**,** 114-122.
527 Ravishankar, H., et al., 2016. Removal of Pb (II) ions using polymer based graphene oxide
528 magnetic nano-sorbent. Process Saf. Environ. 104**,** 472-480.
529 Samuel, M. S., et al., 2018. Adsorption of Pb (II) from aqueous solution using a magnetic
530 chitosan/graphene oxide composite and its toxicity studies. International journal of biological
531 macromolecules 115**,** 1142-1150.
532 Sharififard, H., Soleimani, M., 2017. Modeling and experimental study of vanadium adsorption
533 by iron-nanoparticle-impregnated activated carbon. Res. Chemical Intermediat. 43**,** 2501-2516.
534 Shi, H., et al., 2014. Methylene blue adsorption from aqueous solution by magnetic
535 cellulose/graphene oxide composite: equilibrium, kinetics, and thermodynamics. Ind. Eng. Chem.
536 Res. 53**,** 1108-1118.

Silva, V., et al., 2013. Synthesis and characterization of Fe_3O_4 nanoparticles coated with fucan polysaccharides. J. Magn. Magn. Mater. 343**,** 138-143.

Singh, R., Misra, V., 2015. Stabilization of Zero-Valent Iron Nanoparticles: Role of Polymers and Surfactants. In: M. Aliofkhazraei, (Ed.), Handbook of Nanoparticles. Springer International Publishing, Cham, pp. 1-18.

Smith, E. L., et al., 2014. Deep Eutectic Solvents (DESs) and Their Applications. Chem. Rev. 114**,** 11060-11082.

Stobinski, L., et al., 2014. Graphene oxide and reduced graphene oxide studied by the XRD, TEM and electron spectroscopy methods. J. Electron Spectrosc. 195**,** 145-154.

Thu, T. V., Sandhu, A., 2014. Chemical synthesis of Fe_3O_4–graphene oxide nanohybrids as building blocks for magnetic and conductive membranes. Mater. Sci. Eng. B. 189**,** 13-20.

Tomé, L. I., et al., 2018. Deep eutectic solvents for the production and application of new materials. Appl. Materi. Today. 10**,** 30-50.

Tran, H. V., et al., 2017. Graphene oxide/Fe_3O_4/chitosan nanocomposite: a recoverable and recyclable adsorbent for organic dyes removal. Application to methylene blue. Mater. Res. Express 4**,** 035701.

Wang, H., et al., 2015. Facile synthesis of polypyrrole decorated reduced graphene oxide–Fe_3O_4 magnetic composites and its application for the Cr (VI) removal. Chem. Eng. J. 262**,** 597-606.

Xu, P., et al., 2012. Use of iron oxide nanomaterials in wastewater treatment: A review. Sci. Total Environ. 424**,** 1-10.

Yan, W., et al., 2013. Iron nanoparticles for environmental clean-up: Recent developments and future outlook. Environ. Sci. Proc. Impacts. 15**,** 63.

559 Yang, K., et al., 2010. Re-examination of characteristic FTIR spectrum of secondary layer in
560 bilayer oleic acid-coated Fe_3O_4 nanoparticles. Appl. Surf. Sci. 256**,** 3093-3097.
561 Yang, S., et al., 2015. Preparation of graphene oxide decorated Fe_3O_4@ SiO_2 nanocomposites with
562 superior adsorption capacity and SERS detection for organic dyes. J. Nanomater. 16**,** 337.
563 Zhang, Q., et al., 2019. A novel hierarchical stiff carbon foam with graphene-like nanosheet
564 surface as the desired adsorbent for malachite green removal from wastewater. Environ. Res. 179**,**
565 108746.

566